



Spin–Lattice Relaxation and Diffusion Processes in Aqueous Solutions of Gadolinium-Based Upconverting Nanoparticles at Different Magnetic Fields

Kristina Kristinaityte¹ · Tomasz Zalewski² · Marek Kempka² ·
Simas Sakirzanovas³ · Dovile Baziulyte-Paulaviciene³ · Stefan Jurga² ·
Ricardas Rotomskis^{1,5} · Nomedas R. Valeviciene⁴

Received: 17 September 2018 / Revised: 16 November 2018 / Published online: 14 December 2018
© Springer-Verlag GmbH Austria, part of Springer Nature 2018

Abstract

We investigated the influence of gadolinium (Gd)-based upconverting nanoparticles (UCNPs) on water spin–lattice relaxation (T_1) and diffusion at different magnetic field strengths (0.4 T and 9.4 T). Our findings show that smaller NPs (12 nm compared to 19 nm) were more favourable for proton relaxivity. We also demonstrate that using simplified Solomon–Bloembergen–Morgan (SBM) model we can associate two measured diffusion coefficients with processes occurring near the surface of UCNPs and in bulk water. Using the relationship between relaxation and diffusion, we can estimate not only the total impact of NPs on relaxation of water molecules, but also the impact on relaxation of local water molecules, directly connected to paramagnetic Gd^{3+} ions in NPs. Different magnetic field strengths did not alter the spin–lattice relaxivity of NPs. This suggests that Gd-based UCNPs could be developed into high-performance multimodal magnetic resonance imaging contrast agents working over a broad range of imaging field strengths used in clinical routine.

✉ Kristina Kristinaityte
kkristinaityte@gmail.com

¹ Faculty of Physics, Vilnius University, Sauletekio 9-3, 10222 Vilnius, Lithuania

² NanoBioMedical Center, Adam Mickiewicz University, Umultowska 85, 61-614 Poznan, Poland

³ Faculty of Chemistry and Geosciences, Vilnius University, Naugarduko 24, 10222 Vilnius, Lithuania

⁴ Faculty of Medicine, Vilnius University, Santariskiu 2, 08661 Vilnius, Lithuania

⁵ Laboratory of Biomedical Physics, National Cancer Institute, Vilnius, Lithuania

1 Introduction

Imaging methods have an important role in the management of patient's health care. Some of the advantages made magnetic resonance imaging (MRI) as an exclusive modality. In addition to regular anatomical MRI, other unique contrast mechanisms such as diffusion-weighted imaging (DWI) [1], perfusion-weighted imaging (PWI) [2], magnetic resonance spectroscopic imaging (MRSI) [3] and functional MRI (fMRI) [4] have revolutionized the use of MRI in the clinics. These techniques provide great insight into physiologic mechanisms and pathologic conditions, tracing the links between tissue microstructure, metabolism, and hemodynamics. Contrast agents (CAs) can be used to further improve the sensitivity and detection capability of MRI.

Developments in scanner hardware, image acquisition techniques and reconstruction methods have stimulated MRI to evolve to magnetic fields of higher strength [5]. However, it is well known that longitudinal (r_1) relaxivity of most common gadolinium (Gd)-based commercial contrast agents typically decreases with increasing magnetic field [6–8]. Thus there is an ongoing need to create new contrast agents.

In the last decades different kinds of nanoparticles have attracted significant attention as potential imaging probes. In our paper we study the novel upconverting Gd-containing nanoparticles (UCNPs). The main advantage of these NPs is that they can be used as multimodal contrast agents for MRI and optical imaging.

Upconverting nanoparticles (UCNPs) are inorganic crystalline nanomaterials that can convert near-infrared (NIR) excitation light into visible and ultraviolet emission light. Excitation with NIR light minimizes autofluorescence background and enables deeper penetration into biological samples due to reduced light scattering.

Adding gadolinium into the UCNP turns such a compound into a paramagnetic system, which can be used as MRI contrast agent. Water molecules interact with unpaired electrons of the paramagnetic ion, resulting in a reduction of the proton spin–lattice relaxation time, which means that water proton relaxivity is increased [9].

Typically, three techniques are applied for obtaining high-relaxivity CAs at the nanoscale: size control, surface modification and shape regulation. It has been widely known that the coating layers of UCNPs enhance their fluorescent intensities [10–12]. However, the main challenge remains: how to optimize the NPs' structure and size to achieve the most efficient relaxivity without loss of their optical properties.

When surfactant molecules are used, they interact with water, hence diffusion of water molecules must decelerate. That affects the behaviour of the spins, if the external magnetic field is inhomogeneous. This is the reason why diffusion measurements can give fundamental details of such system when effectiveness of MRI contrast agent is concerned.

The goal of our work is to investigate the influence of different sized Gd-based upconverting nanoparticles on water diffusion and spin–lattice relaxation at different magnetic field strengths. Understanding these processes would help us to better understand the key factors enhancing the relaxation of contrast agents.

2 Materials and Methods

2.1 Mechanisms of Spin–Lattice Relaxation

For spins-1/2, relaxation is caused by fluctuating magnetic fields at the sites of the nuclear spins, caused by thermal motion of the molecules. There are different sources of local magnetic fields, but in most experimental cases, a single relaxation mechanism dominates. For spins-1/2 it is usually dipole–dipole mechanism.

The relaxation mechanism of electron–nuclear magnetic interaction in paramagnetic systems is usually explained by Solomon–Bloembergen–Morgan (SBM) model using three sub-systems (Fig. 1) [13, 14]: the water molecules that bind directly to the gadolinium ion forming the first coordination shell, water molecules with protons that make up the long-lived second coordination shell and water molecules that move in the bulk. For the MRI contrast agents, a simpler SBM model of two spheres is more often used [15]. Such relaxation mechanism, including an inner-sphere and an outer-sphere component, will be used later in our study.

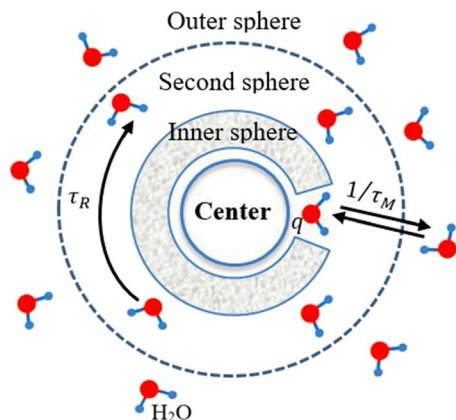
The longitudinal relaxation rate ($1/T_1^{\text{dip}}$) that takes place in the first sub-system is described by spin–electron interaction given by Eq. (1) [13]:

$$\frac{1}{T_1^{\text{dip}}} = R_1^{\text{dip}} = \frac{2}{15} \cdot \frac{\gamma_1^2 g^2 \mu_B^2 S(S+1)}{r_{\text{GdH}}^6} \left(\frac{\mu_0}{4\pi}\right)^2 \cdot \left[\frac{3\tau_{c1}}{1 + \omega_1^2 \tau_{c1}^2} + \frac{7\tau_{c2}}{1 + \omega_S^2 \tau_{c2}^2} \right]. \quad (1)$$

Here, S is the electron spin quantum number, γ_1 is the nuclear gyromagnetic ratio, g is the electron g -factor, μ_B is the Bohr magneton, r_{GdH} is the distance between Gd^{3+} and the water proton, μ_0 is the magnetic permeability of a vacuum, ω_1 and ω_S are the nuclear and electron Larmor frequencies, τ_{c1} and τ_{c2} are the correlation times of nuclear and electron motion, respectively.

Spin–lattice relaxation rate ($R_1 = 1/T_1$) of a nuclear spin that interacts with unpaired electron spin of a paramagnetic ion is proportional to the inversed sixth power of the distance between the water proton and paramagnetic ion. This is why processes around the surface of the NPs are at the first importance. Water

Fig. 1 Inner sphere, secondary sphere, and outer sphere of the Solomon–Bloembergen–Morgan (SBM) relaxation model [13, 16]



molecules that are directly coordinated to the paramagnetic center are responsible for the inner-sphere relaxation contribution, while bulk water molecules in the nearby environment affect outer-sphere relaxation.

On the basis of the SBM theory, common strategies for enhancing spin lattice relaxivity mainly include increasing the number of bound water molecules (q), enhancing rotational correlation time (τ_R) and optimizing water residence time (τ_M). Higher τ_R values imply slower molecular tumbling and lead to increased proton relaxivity. τ_M is the inverse of water exchange rate in the inner sphere [16].

Comparing the effectiveness of contrast agents, relaxivity (r_1) is the main parameter. It is defined as the slope of a plot of relaxation rate ($1/T_1$) versus concentration of contrast agent (CA):

$$\frac{1}{T_1} = \frac{1}{T_{10}} + r_1 C. \quad (2)$$

Here T_{10} is the relaxation time of the sample in the absence of the contrast agent and C is the concentration of CA (mM).

2.2 Sample Preparation

In this study, core and core-shell UCNP were synthesized via a thermal decomposition method as published in the co-authors article [17]. Hexagonal phase β -NaGdF₄ was chosen as host lattice for its ability to combine optical and magnetic properties [18]. The mean diameter of the synthesized NaGdF₄:Yb, Er core nanoparticles and core-shell nanoparticles with NaGdF₄ optical inert layer covering the NaGdF₄:Yb, Er was 12 nm and 19 nm, respectively (Fig. 2).

The size of nanoparticles was confirmed by transmission electron microscopy (TEM). Experiments were carried out using high-resolution (maximum resolution: 0.63 Å) transmission electron microscope HRTEM Jeol ARM 200F in NanoBioMedical center, AMU, Poznan.

Both kinds of hydrophobic UCNP were converted into hydrophilic ones using a nonionic surfactant polysorbate 80 (Tween 80, polyoxyethylene sorbitan laurate). Tween 80 was used to make the UCNP colloidal stable and dispersible in water while protecting the surface from non-specific adsorption of biomolecules.



Fig. 2 Schematic presentation of two kinds of UCNP both functionalized with surfactant TWEEN80: 12 nm NaGdF₄:Yb, Er core and 19 nm NaGdF₄:Yb, Er@NaGdF₄ core-shell, where the 12 nm core was additionally coated with 7 nm of NaGdF₄ optical inert layer

2.3 NMR Spectroscopy

^1H -NMR spectra, spin–lattice relaxation times T_1 and diffusion rates have been measured at 37 °C on Bruker AVANCE III HD spectrometer operating at resonance frequency of 400 MHz (magnetic field of 9.4 T). For comparison, measurements were also carried out on the homemade spectrometer operating at resonance frequency of 16 MHz (magnetic field of 0.4T). Samples of two different contrast agents were placed in 5 mm NMR tubes with capillary of DSS and D_2O for referencing and shimming the magnet.

For calculation of relaxivities, at least four different concentrations of each CA were measured. For T_1 measurements an inversion-recovery pulse sequence was employed using 16 increments with two scans each and the relaxation delay was set to $5T_1$. The 90° pulse length was approximately 24 μs and was adjusted for each experiment.

A pseudo-2D diffusion experiments were carried out using stimulated echo sequence with 1 spoil gradient. Instead of incrementing a delay, the gradient strength was incremented from 2% to 95% in 64 steps.

During the diffusion experiment, the intensity of NMR signal depends on diffusion coefficient (D) as in Eq. (3):

$$I \sim \exp \left[-(\gamma G \delta)^2 D \left(\Delta - \frac{\delta}{3} \right) \right], \quad (3)$$

where γ is the gyromagnetic ratio and G is the gradient strength. The diffusion time (Δ) and diffusion gradient length (δ) were 130 ms and 2 ms, respectively. Knowing all the constants we can easily calculate the diffusion coefficient using the slope of the intensity dependence on the squared gradient strength.

NMR spectra, relaxation times and diffusion rates were processed using Topspin 3.2 software. Additionally the signal shapes and relaxivity calculations were processed using Microcal Origin 9 package.

3 Results and Discussion

3.1 Size of Nanoparticles

TEM images showed the expected values of size of our nanoparticles. The mean diameters of core and core–shell UCNPs were 12 nm and 19 nm, respectively. The results are presented in Fig. 3.

3.2 Spin–Lattice Relaxation

We started the experiments by measuring T_1 of bulk water that was used to prepare different concentrations of our contrast agents. The obtained value of

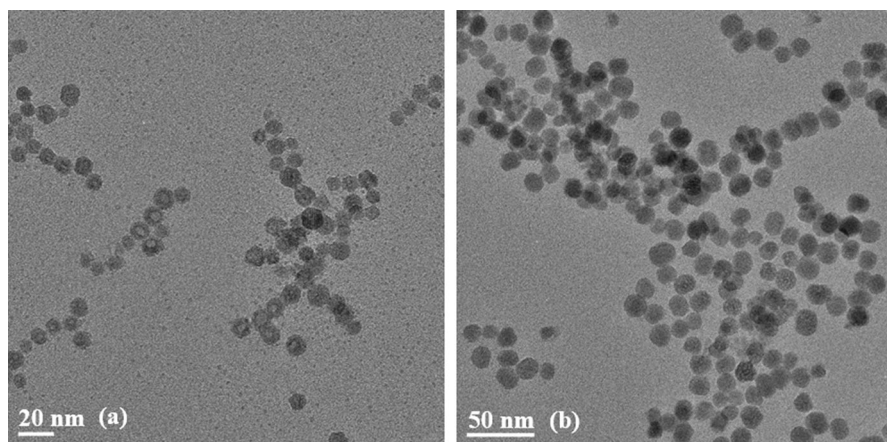


Fig. 3 TEM images of two different UCNPs: 12 nm NaGdF₄:Yb, Er core (a) and 19 nm NaGdF₄:Yb, Er@NaGdF₄ core-shell (b)

relaxation rate ($R_1 = 0.26 \text{ s}^{-1}$ at $37 \text{ }^\circ\text{C}$) was later needed for the calculations of relaxivities (Eq. (2)) of our analyzed samples. The measured T_1 value of water was in good agreement with the ones from literature [19, 20].

The results showed that relaxivity of our CAs increased from $0.684 \text{ mM}^{-1} \text{ s}^{-1}$ for 19 nm NPs to $0.986 \text{ mM}^{-1} \text{ s}^{-1}$ for the 12 nm ones. According to the literature [21–24], for T_1 contrast agents, small-sized NPs usually generate greater contrast enhancement. Several research groups reported similar size effects of NaGdF₄ NPs on relaxivity. Correlations of NPs' sizes and their relaxivities showed that contributions from the surface-to-volume ratio increased with decreasing NP size, becoming the dominant contributing factor.

However, Gao and co-workers demonstrated that larger NPs possessed higher r_1 value. It was explained by saying that τ_R became lower for larger NPs ($> 15 \text{ nm}$) and played a dominant role in affecting relaxivity [25]. In our case, even if the size of NPs reached 19 nm, the results showed that we were still in a range where surface-to-volume ratio was the dominant contributing factor.

All research groups mentioned above, worked with magnetic fields of less than 3T, which is the most common magnetic field strength applied in clinical routine. Our spectrometer was operating at resonance frequency of 400 MHz. For comparison we decided to measure r_1 values of our NPs at the 0.4 T magnetic field as well. The summarized results of T_1 measurements of two different sized nanoparticles at two different magnetic field strengths are shown in Fig. 4.

It is well known that the spin–lattice relaxivity for Gd-based CA typically decreases with increasing magnetic field [6–8]. However, no significant difference in relaxivity, comparing the r_1 values measured at 16 MHz and 400 MHz, was noticed.

Fig. 4 Spin–lattice relaxation rates in aqueous solutions of different-sized β -NaGdF₄ nanoparticles (12 nm core and 19 nm core–shell) as a function of concentration of Gd³⁺ ions at a temperature of 37 °C

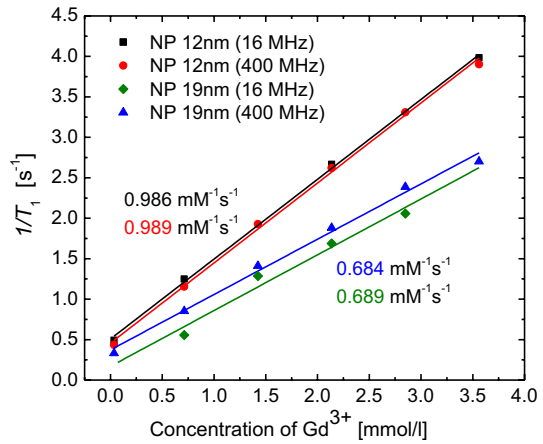
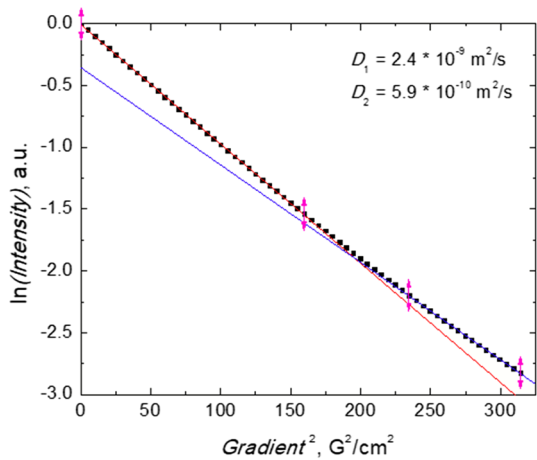


Fig. 5 Signal decay of aqueous solution of 19 nm core–shell NPs versus squared gradient strength. Two separate diffusion coefficients (D_1 and D_2) were calculated by fitting



3.3 Diffusion Experiments

The results of NMR diffusion for core–shell 19 nm NPs are demonstrated in Fig. 5. Instead of one diffusion constant, as expected in most NMR cases, we got two (D_1 and D_2) with different contributions (around 96% and 4%, respectively) to the total intensity of NMR signal (Fig. 5).

For further analysis of two diffusion coefficients, we measured their dependence on the temperature at two different concentrations (1 g/l and 0.75 g/l) (Fig. 6). Using the Arrhenius plot we then could calculate the activation energies. The activation energy can also be calculated from the relaxation measurements, having the temperature-dependent R_1 values.

We found that one diffusion coefficient was concentration-dependent, while the other one remained the same for both concentrations. Moreover, the activation energy of pure water, calculated using the results from relaxation experiments

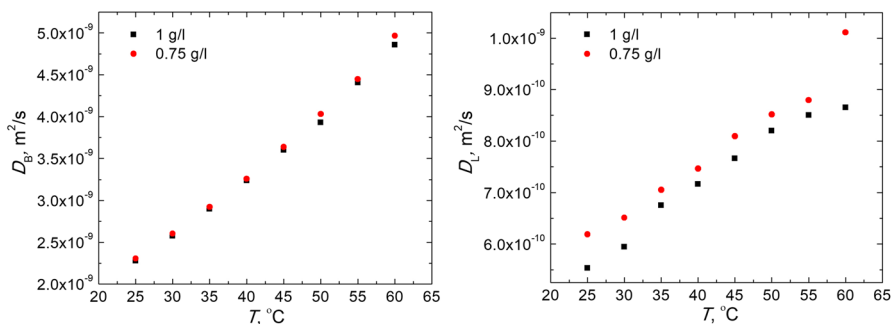


Fig. 6 Temperature-dependent diffusion coefficients of bulk water D_B (left) and local water D_L (right) for 19 nm core-shell NPs of different concentrations

(20.442 kJ/mol), was comparable to the activation energy of water in NPs samples, calculated using the temperature dependence of D_1 values (21.362 kJ/mol).

On the basis of the obtained results, for the later analysis we will use the simplified SBM model assuming that there are only two processes involved in the relaxation mechanism. One of them will reflect the behaviour of bulk water having the diffusion coefficient D_B (instead of previously used D_1). The other one will represent local water (water molecules that interact with Gd^{3+} ion directly) having the diffusion coefficient D_L (instead of D_2). Then the total relaxation rate can be written as:

$$R_1 = R_{1B} \cdot I_B + R_{1L} \cdot I_L. \quad (4)$$

Here I_B and I_L are the contributions of bulk and local water diffusion in CA samples to the total signal intensity. Their values were given by the Topspin 3.2 software together with the calculated diffusion coefficients. If we change the relaxation rate of bulk water (R_{1B} value) to the relaxation rate of pure water, we can calculate the relaxation rate of local water at the surface of NPs, because all the other parameters are known.

This relationship between relaxation and diffusion opens more possibilities to investigate water molecules near the surface of UCNPs, which deepens our understanding of key factors influencing the relaxivity of contrast agents.

4 Concluding Remarks

Strategies to achieve high relaxivity of MRI spin-lattice contrast agents mainly focus on enhancing the interaction between NPs and nearby water protons. Our study demonstrated that the diffusion processes of water, measured by NMR spectroscopy, might be related to the SBM model, which is used for explaining relaxation mechanisms of MRI contrast agents. Using such relationship we can calculate not only the total impact of NPs on relaxation of water molecules, but also the impact on relaxation of local water molecules, directly connected to paramagnetic Gd^{3+} ions in NPs. An in-depth understanding of these processes can guide the engineering of future NPs by finding the most optimal structure for the enhancement of spin-lattice relaxation.

The next generation of MRI CAs is being developed based not only on the design principles of NPs, but also on the development of advanced nanotechnology, novel MRI techniques and new clinical applications. This is why it would be valuable to design multimodal contrast agents that have excellent relaxation properties over a broad range of imaging field strengths and are characterized by effective upconversion properties.

On the basis of our results, we believe that Gd-based UCNPs could be developed into high-performance multimodal MRI contrast agents.

Acknowledgements One of us (K.K.) thanks for the hospitality of Prof. Dr. Stefan Jurga group in NanoBio-Medical Center, Poznan, where the part of the experiments were carried out. Special thanks to Dr. Grzegorz Nowaczyk for the TEM measurements and Prof. Dr. Vytautas Balevicius and Laurynas Dagys for their help during the experiments and discussions.

References

1. S.C. Partridge, N. Nissan, H. Rahbar, A.E. Kitsch, E.E. Sigmund, *JMRI* **45**, 337–355 (2017)
2. A.M. Priola, S.M. Priola, D. Gned, E. Piacibello, D. Sardo, G. Parvis, D. Torti, F. Ardissonne, A. Veltri, *JMRI* **44**, 758–769 (2016)
3. S. Verma, A. Rajesh, J.J. Fütterer, B. Turkbey, T.W.J. Scheenen, Y. Pang, P.L. Choyke, J. Kurhanewicz, *AJR* **194**, 1414–1426 (2010)
4. C.M. Rios, M.P. McAndrews, W. Logan, T. Krings, D. Lee, E. Widjaja, *JMRI* **44**, 12–22 (2016)
5. T.F. Budinger, M.D. Bird, L. Frydman, J.R. Long, T.H. Mareci, W.D. Rooney, B. Rosen, J.F. Schenck, V.D. Schepkin, A.D. Sherry, D.K. Sodickson, C.S. Springer, K.R. Thulborn, K. Ugurbil, L.L. Wald, *Magn. Reson. Mater. Phys.* **29**, 617–639 (2016)
6. P. Caravan, ChT Farrar, L. Frullano, R. Uppal, *Contrast. Media Mol. Imaging* **4**(2), 89–100 (2009)
7. V. Jacques, S. Dumas, WCh. Sun, J.S. Troughton, M.T. Greenfield, P. Caravan, *Invest. Radiol.* **45**(10), 613–624 (2010)
8. M. Rohrer, H. Bauer, J. Mintorovich, M. Requardt, H.J. Weinmann, *Invest. Radiol.* **40**, 715–724 (2005)
9. A.M. Panich, N.A. Sergeev, *Appl. Magn. Reson.* **49**, 195–208 (2018)
10. F.C.J.M. van Veggel, C. Dong, N.J.J. Johnson, J. Pichaandi, *Nanoscale* **4**, 7309–7321 (2012)
11. L. Dongdong, S. Qiyue, D. Yan, J. Jianqing, *J. Rare Earths* **32**(11), 1032–1036 (2014)
12. C. Liu, Z. Gao, J. Zeng, Y. Hou, F. Fang, Y. Li, R. Qiao, L. Shen, H. Lei, W. Yang, M. Gao, *ACS Nano* **7**(8), 7227–7240 (2013)
13. G.A. Pereira, C.F.G.C. Geraldes, *Ann. Magn. Reson.* **6**(1/2), 1–33 (2007)
14. R.D.A. Alvares, A. Gautam, R.S. Prosser, F.C.J.M. van Veggel, P.M. Macdonald, *J. Phys. Chem.* **121**, 17552–17558 (2017)
15. V.C. Pierré, S.M. Harris, S.L. Pailloux, *Acc. Chem. Res.* **51**, 342–351 (2018)
16. D. Ni, W. Bu, E.B. Ehlerding, W. Cai, J. Shi, *Chem. Soc. Rev.* **46**, 7438–7468 (2017)
17. D. Baziulyte-Paulaviciene, V. Karabanovas, M. Stasys, G. Jarockyte, V. Poderys, S. Sakirzanovas, R. Rotomskis, *Beilstein J. Nanotechnol.* **8**, 1815–1824 (2017)
18. M. Ding, D. Chen, S. Yin, Z. Ji, J. Zhong, Y. Ni, C. Lu, Z. Xu, *Sci. Rep.* **5**(12745), 1–14 (2015)
19. E. Von Goldammer, H.G. Hertz, *J. Phys. Chem.* **74**, 3734–3755 (1970)
20. V.I. Chizhik, Y.S. Chernyshev, A.V. Donets, V.V. Frolov, A.V. Komolkin, M.G. Shelyapina, *Magnetic Resonance and Its Applications* (Springer, Berlin, 2014) p. 206
21. X.Y. Zheng, K. Zhao, J. Tang, X.Y. Wang, L.D. Li, N.X. Chen, Y.J. Wang, S. Shi, X. Zhang, S. Malaisamy, L.D. Sun, X. Wang, C. Chen, C.H. Yan, *ACS Nano* **11**, 3642–3650 (2017)
22. F. Chen, W. Bu, S. Zhang, X. Liu, J. Liu, H. Xing, Q. Xiao, L. Zhou, W. Peng, L. Wang, J. Shi, *Adv. Funct. Mater.* **21**, 4285–4294 (2011)
23. N.J. Johnson, S. He, V.A. Nguyen Huu, A. Almutairi, *ACS Nano* **10**, 8299–8307 (2016)
24. N.J.J. Johnson, W. Oakden, G.J. Stanis, R.S. Prosser, F.C.J.M. van Veggel, *Chem. Mater.* **23**, 3714–3722 (2011)
25. Y. Hou, R. Qiao, F. Fang, X. Wang, C. Dong, K. Liu, C. Liu, Z. Liu, H. Lei, F. Wang, M. Gao, *ACS Nano* **7**(1), 330–338 (2013)